Supporting Information for

Optimized energy level, morphology and photophysical procedure boosted the photovoltaic performance in monochlorinated benzothiadiazole-based polymer donors

Junfeng Tong*[,a,‡], Wuyan Liu[a,‡], Lili An[b], Shilei Qu[a], Aoxiang Zhang[a], Pengzhi Guo[a], Zezhou Liang[c], Lihe Yan[c], Chunyan Yang[a], Jianfeng Li[a], Yangjun Xia*[,a]

[a] *Gansu Provincial Engineering Research Center for Organic Semiconductor Materials and Application Technology, School of Materials Science and Engineering, Lanzhou Jiaotong University, Lanzhou, 730070*

[b] *School of Chemical Engineering, Northwest Minzu University, Lanzhou 730030, China*

[c] *Key Laboratory for Physical Electronics and Devices of the Ministry of Education & Shaanxi Key Lab of Information Photonic Technique, School of Electronics and Information Engineering, Xi'an Jiaotong University, Xi'an, 710049, China*

E-mail address: tongjunfeng139@163.com (J. Tong), xiayangjun2015@126.com (Y. Xia)

‡These authors contributed to this work equally.

1. EXPERIMENTAL SECTION

Table S1 Bandgap, energy level and device parameters of chlorinated benzothiadiazole-based polymers.

Polymer Donor	Acceptor	E_g^{opt} (eV)	E_{HOMO}/E_{LUMO} (eV)	V_{OC} (V)	J_{SC} (mA cm^{-2})	*FF* (%)	PCE (%)	Ref.
PBDTHD-ClBTDD	$PC_{71}BM$	1.68	–5.53/–3.71	0.76	16.79	71.69	9.11	[1]
PBDTBO-ClBTDD	$PC_{71}BM$	1.70	–5.47/–3.70	0.68	11.69	62.30	4.95	[1]
PBDTHD-ClBTEH	$PC_{71}BM$	1.71	–5.53/–3.71	0.79	13.33	63.12	6.88	[1]
PBDTBO-ClBTEH	$PC_{71}BM$	1.69	–5.50/–3.73	0.78	10.94	64.36	5.46	[1]
PCBT4T-2OD	$PC_{71}BM$	1.59	–5.26/–3.59	0.73	16.18	68.97	8.21	[2]
PCCBT4T-2OD	$PC_{71}BM$	1.61	–5.32/–3.62	0.85	11.93	60.14	6.12	[2]
PBBCl1-T2	$PC_{71}BM$	1.60	–5.49/–3.22	0.87	8.44	49.49	3.64	[3]
PBBCl1-T3	$PC_{71}BM$	1.56	–5.44/–3.38	0.73	13.75	68.59	6.87	[3]
PBBCl2-T3	$PC_{71}BM$	1.59	–5.50/–3.21	0.84	9.90	63.94	5.33	[3]
PCl_1	$PC_{71}BM$	1.48	–5.40/–3.92	0.71	6.5	37	1.88	[4]
PCl_2	$PC_{71}BM$	1.66	–5.56/–3.90	0.92	2.3	28	0.67	[4]
P2	$PC_{71}BM$	1.51	–5.34/–3.73	0.77	10.93	44.90	4.08	[5]
P3	$PC_{71}BM$	1.49	–5.30/–3.68	0.83	9.10	47.69	3.95	[5]

1.1 Measurement and characterization

^{1}H NMR spectra of the intermediates were characterized on a Bruker XRD-500 Spectrometer in $CDCl_3$ solution as standard (Bruker Instruments, Germany). The thermogravimetric weight is measured by using the TG209F3 thermogravimetric analyser (NETZSCH, USA). Optical contact angle measurement on DSA100 surface tension meter (Kruss, Germany). Cyclic voltammetry (CV) was measured on a CHI electrochemical workstation (Shanghai Chenhua, Shanghai, China) at a scan rate of 100 mV s^{-1} with a nitrogen-saturated solution of 0.1 M tetrabutylammonium hexafluorophosphate (Bu_4NPF_6) in CH_3CN solution. Spin-coating various types of coatings on the devices using a KW-4A desktop leveler (Zhangqiu City Guan Brand Company) and testing the film thickness with a film thickness tester (BRUKER, USA). Vaporized the devices using vacuum coating instrument of model SZZ450 (Shenyang New Blue Sky Vacuum Technology). The devices were irradiated with a solar simulator (San-Ei Electric, Japan) and various important parameters of the PV devices were measured by a solar J-V test system (Keithley, USA). Characterization of the EQE of the device on a 7-SCSpecIII external quantum efficiency measurement instrument (Seven Star Optical Instruments, Beijing, China)。

1.2 Fabrication of organic solar cell and mobility characterization

The device with the structure of ITO/PEDOT:PSS/active layer/PDINN/Al (Fig. S1) was fabricated as following. Indium tin oxide (ITO) coated glass substrates were washed by a wet-cleaning process inside an ultrasonic bath, with de-ionized water, acetone, de-ionized water and isopropanol in turn. After drying under nitrogen flow, the substrates were treated with oxygen plasma for 10 min, then a thin layer of poly(3,4-ethylenedioxythiophene): poly(styrene-sulfonate) (PEDOT:PSS, *ca*. 40 nm, Clevios PVP Al4083) was spin-coated onto the ITO substrates and annealed at 150 ºC for 20 min. After that the substrates were transferred into a nitrogen-filled glove box and the active layer was prepared. The active layer, with a thickness in the 100~120 nm range, was deposited on top of the PEDOT:PSS layer by spin-casting from chloroform solution containing the studied materials. The thickness of the active layer was verified by a surface profilometer (DektakXT, Bruker). Then, an ultrathin layer of PDINN (1 $mg \cdot mL^{-1}$ in methanol) was spin-coated on the active layer. Finally, the Al layer (~55 nm) as the cathode was thermally evaporated under a vacuum pressure of 10^{-4} Pa. Moreover, each device had 5 cells and the each effective cell area in this work was 0.1 cm^2, which was ascertained by a shadow mask (fingers fashion). The thickness values of the evaporated Al was monitored by a quartz crystal thickness/ratio monitor (SI-TM206, Shenyang Sciens Co.). The PCEs of the resulting PSCs were measured under 1 sun, AM 1.5 G (Air mass 1.5 global) condition using a solar simulator (XES-70S1, San-EI Electric Co.) with irradiation of 100 $mW \cdot cm^{-2}$. The current density-voltage (*J-V*) characteristics were recorded with a Keithley 2400 source-measurement unit. The spectral responses of the devices were measured with a commercial external quantum efficiency (EQE)/incident photon to charge carrier efficiency (IPCE) setup (7-SCSpecIII, Beijing 7-star Opt. In. Co.) equipped with a standard Si diode.

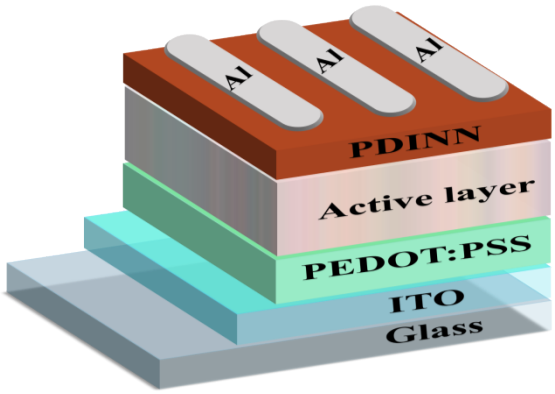

Fig. S1 The device architecture of the organic solar cell in our study.

The hole-only and electron-only devices were prepared with a diode configuration of

ITO/PEDOT:PSS/active layer/MoO_3/Ag or ITO/ZnO/active layer/PDINN/Ag, respectively. The device characteristics were extracted by modeling the dark current under an applied forward bias. The hole and electron mobilities of the active layers were extracted by fitting the current-voltage curves using the Mott-Gurney relationships (space-charge-limited-current, SCLC). The field dependent SCLC behavior can be expressed as: $J = \frac{9}{8}\varepsilon_0\varepsilon_r\mu\frac{V^2}{L^3}$. Where J stands for the current density, ε_0 is the permittivity of free space (8.85×10^{-12} F·m^{-1}), ε_r is the relative permittivity of the transport medium (assumed to be 3, which is a typical value for CPs), μ is the zero-field mobility of hole or electron, L is the thickness of the active layer, and effective voltage $V = (V_{appl} - V_{bi})$, where V_{appl} is the applied voltage to the device and V_{bi} is the built-in voltage. By linearly fitting $J^{1/2}$ with V, the mobilities were extracted from the slope and L: $\mu = \frac{slope^2 \times 8L^3}{9\varepsilon_0\varepsilon_r}$. For the hole-only devices, V_{bi} is 0 V, while V_{bi} = 0.7 V in the electron-only devices.

1.3 Surface energy calculation

The surface tension (γ) can be evaluated using the Wu model, *via* Equations (1), (2), and (3), on the basis of the measured contact angles (θ) information.

$$\gamma_{water}(1 + cos\Theta_{water}) = \frac{4\gamma_{water}^{d}\gamma^{d}}{\gamma_{water}^{d} + \gamma^{d}} + \frac{4\gamma_{water}^{p}\gamma^{p}}{\gamma_{water}^{p} + \gamma^{p}} \quad (1)$$

$$\gamma_{EG}(1 + cos\theta_{EG}) = \frac{4\gamma_{EG}^{d}\gamma^{d}}{\gamma_{EG}^{d} + \gamma^{d}} + \frac{4\gamma_{EG}^{p}\gamma^{p}}{\gamma_{EG}^{p} + \gamma^{P}} \quad (2)$$

$$\gamma = \gamma^{d} + \gamma^{p} \quad (3)$$

Where, γ is the surface energy of the studied semiconductor; γ^d and γ^p are the dispersion and polar components of γ; γ_i is the total surface energy of the i material (i = water or ethylene glycol); γ_i^d and γ_i^p are the dispersion and polar components of γ_i; and θ is the droplet contact angle (water or ethylene glycol) on the semiconductor film. Flory-Huggins interaction parameter $\chi^{donor-acceptor}$, which is a parameter to evaluate the interaction between polymer donors and acceptor Y6, based on this, the miscibility of the two components can be objectively judged. The smaller the difference of surface energy between donor and acceptor, the lower the value of $\chi^{donor-acceptor}$ and the better the miscibility.

1.4 Femtosecond time-resolved Transient Absorption (fs-TA) Measurements

Fs-TA spectroscopy was performed to measure the temporal evolution of the absorption changes in the excited states, through which the carrier dynamics in femtosecond to nanosecond regime could be revealed. The laser beam is supplied by amplified Ti: sapphire laser source (800 nm, Coherent) that provides 100 fs pulses with a repetition rate of 1 kHz. The output was split into two beams, the stronger one of which was frequency doubled to generate a 400 nm pump light, and the other one was focused into a sapphire plate to generate a broadband supercontinuum probe light. Using an optical chopper, the repetition rate of the pump pulses was adjusted to 500 Hz, and were focused on the sample with the probe pulse (white light). The TA spectra were obtained by comparing the probe light spectra with and without pump light excitation. The photo-induced absorption change as a function of wavelength was described using optical density (absorbance) changes ($\Delta OD(\lambda)$). By adjusting the delay time between the pump and probe pulses, a 3D transient spectral image $\Delta OD(\lambda,t)$ was formed.

2. Supplementary Figures and Tables

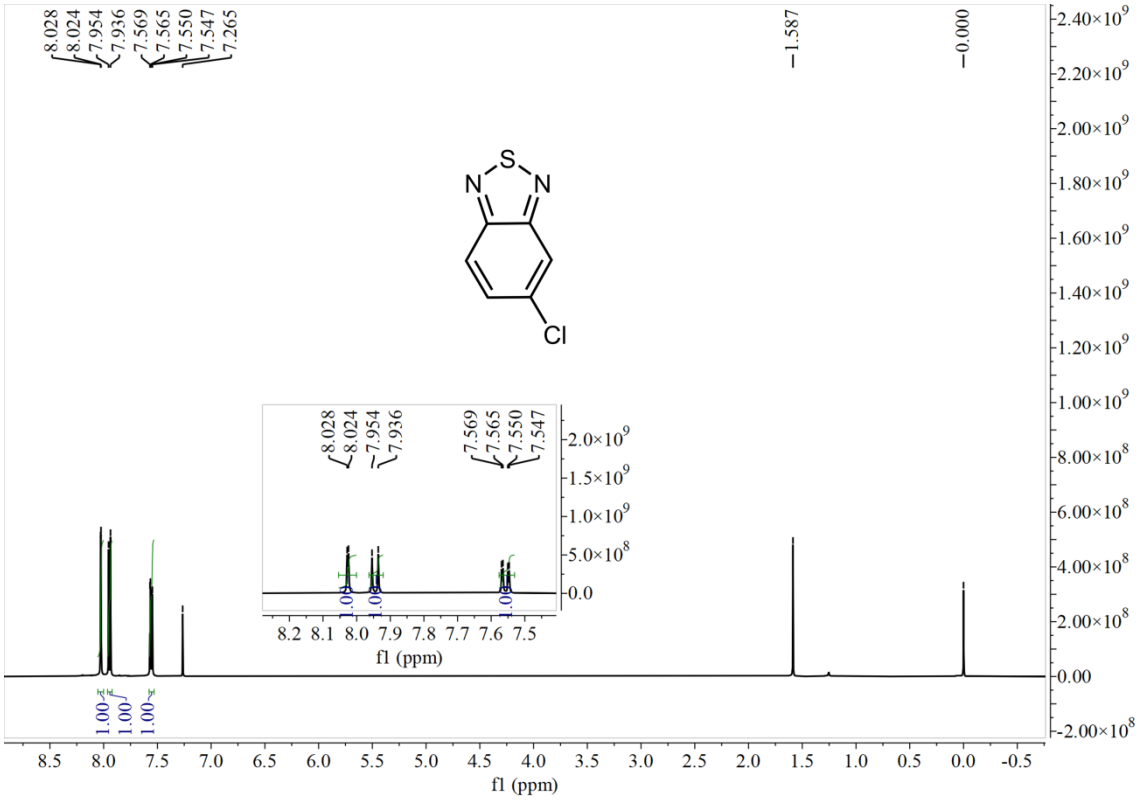

Fig. S2. ^{1}H NMR spectrum of ClBT in $CDCl_3$.

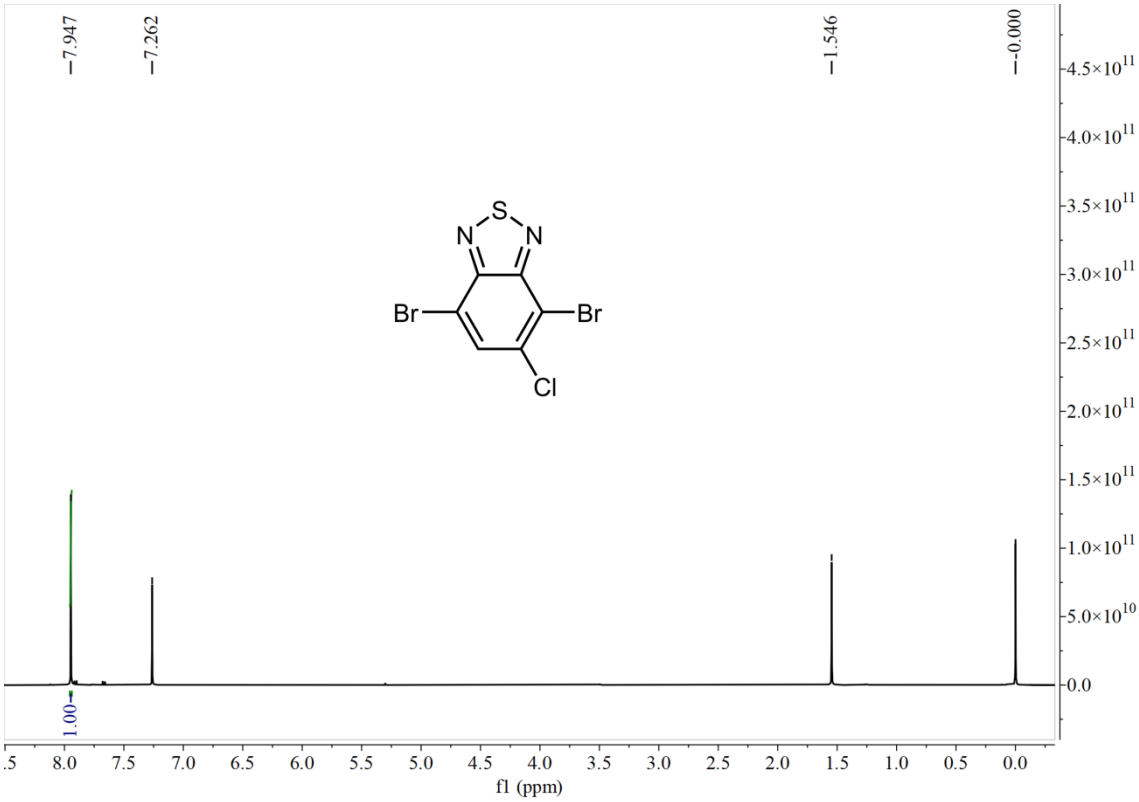

Fig. S3. ^{1}H NMR spectrum of $ClBTBr_2$ in $CDCl_3$.

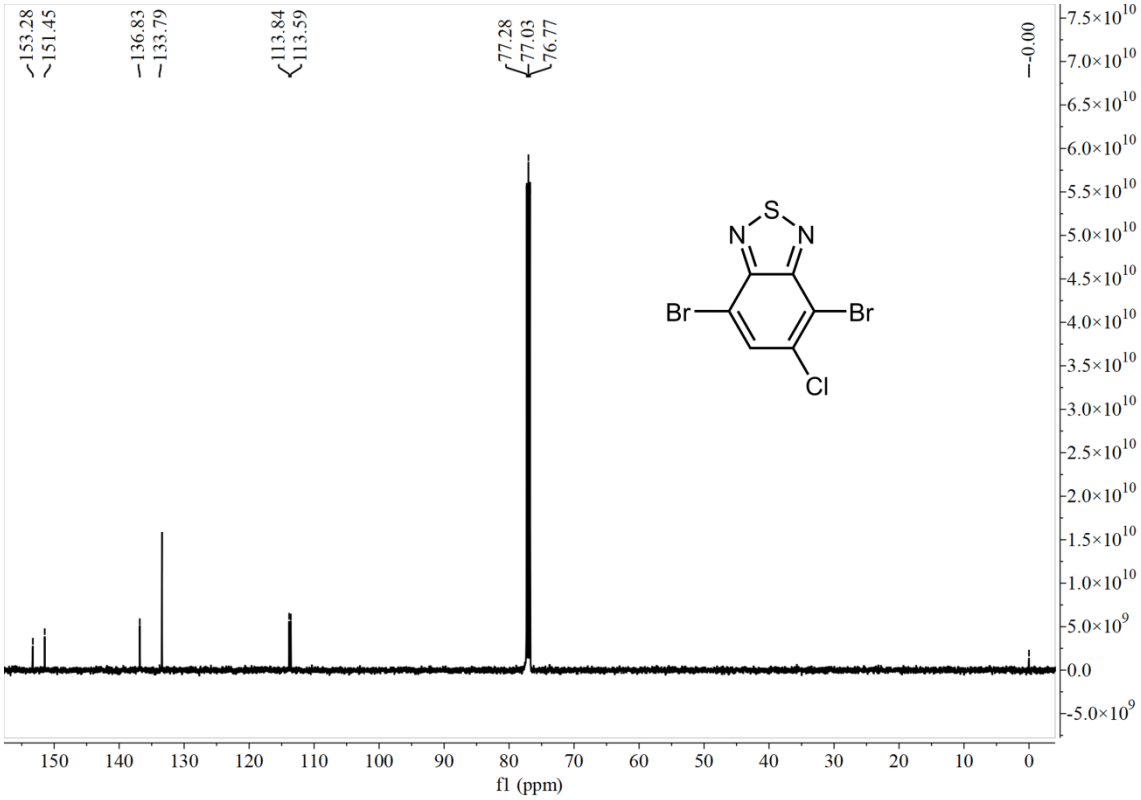

Fig. S4. ^{13}C NMR spectrum of $ClBTBr_2$ in $CDCl_3$.

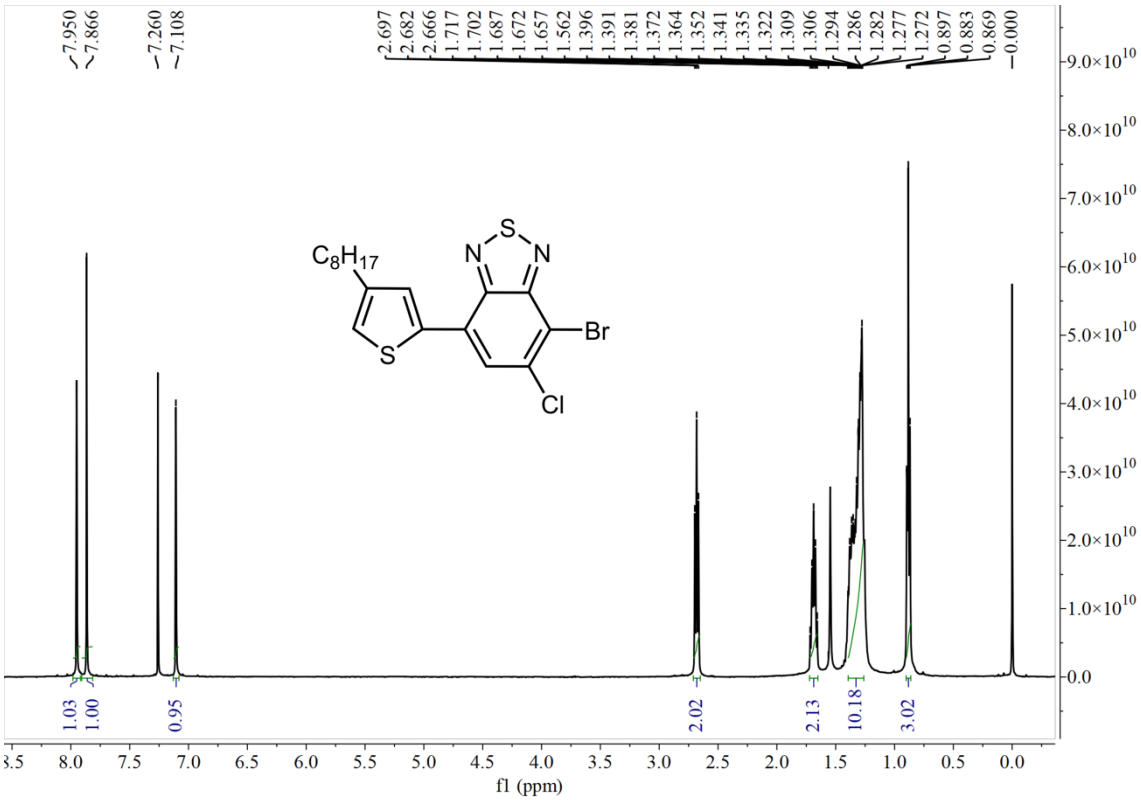

Fig. S5. ^{1}H NMR spectrum of TClBTBr in $CDCl_3$.

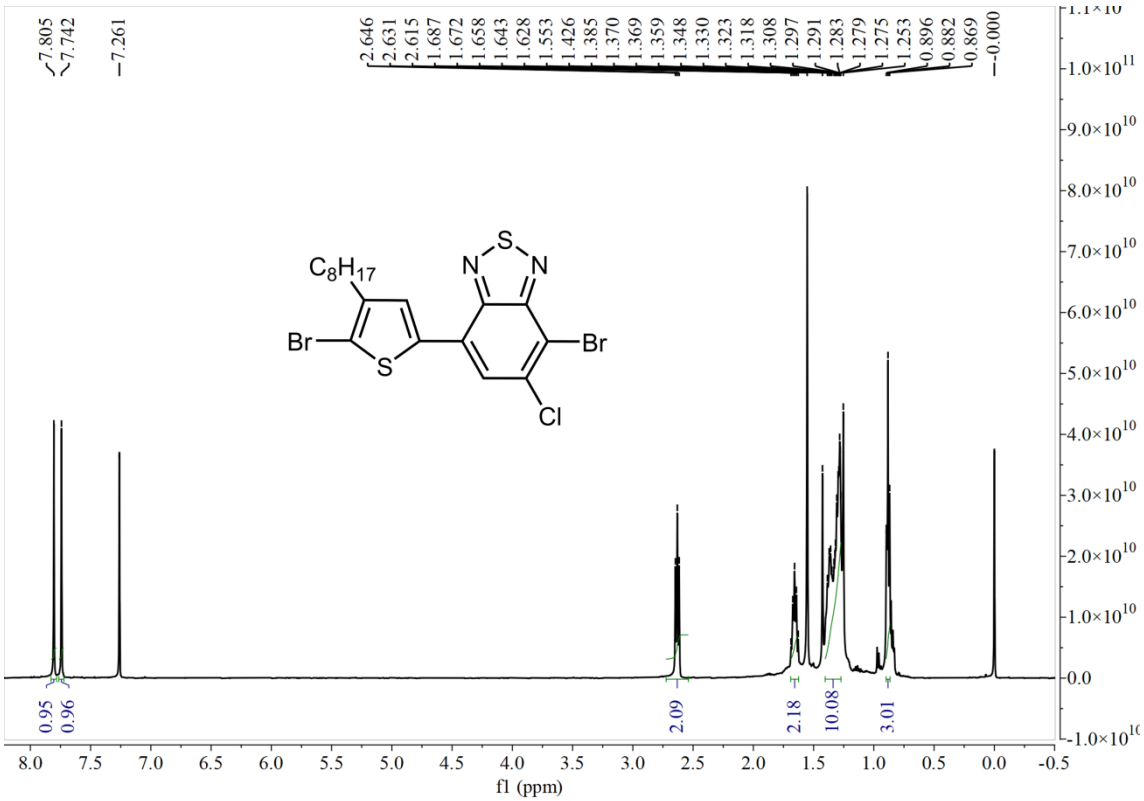

Fig. S6. ^{1}H NMR spectrum of TClBTBr$_2$ in CDCl$_3$.

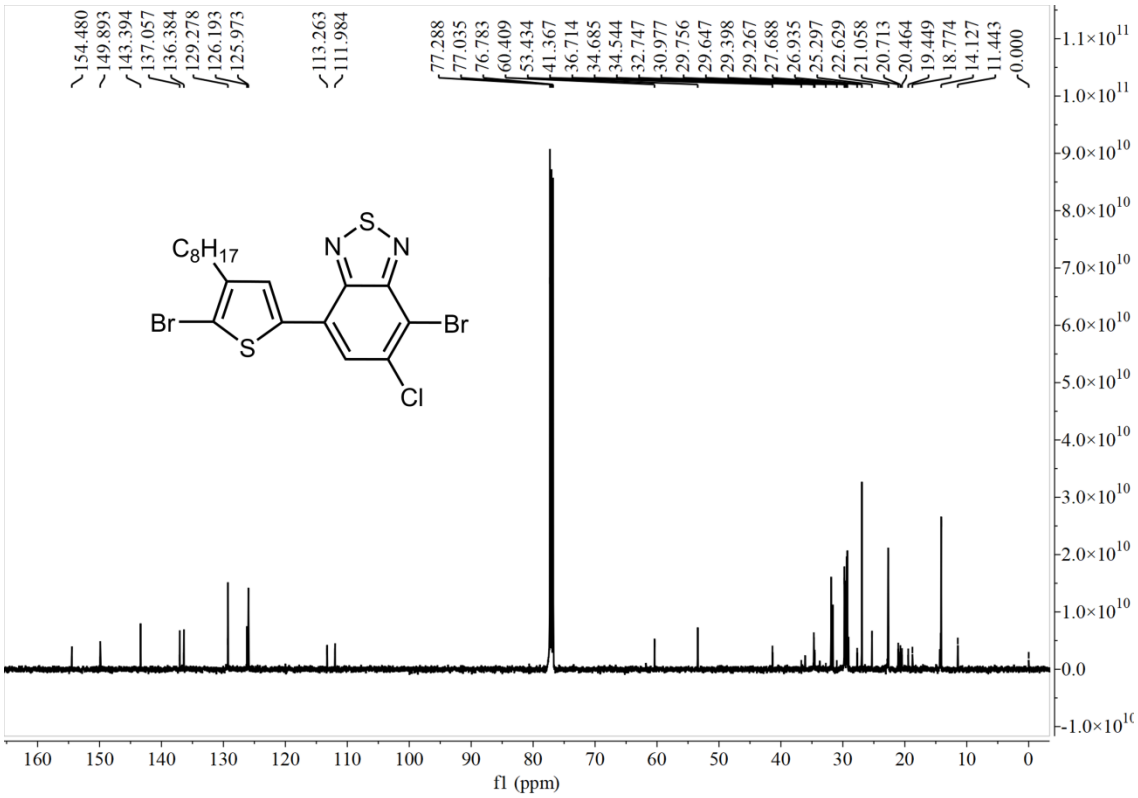

Fig. S7. ^{13}C NMR spectrum of TClBTBr$_2$ in CDCl$_3$.

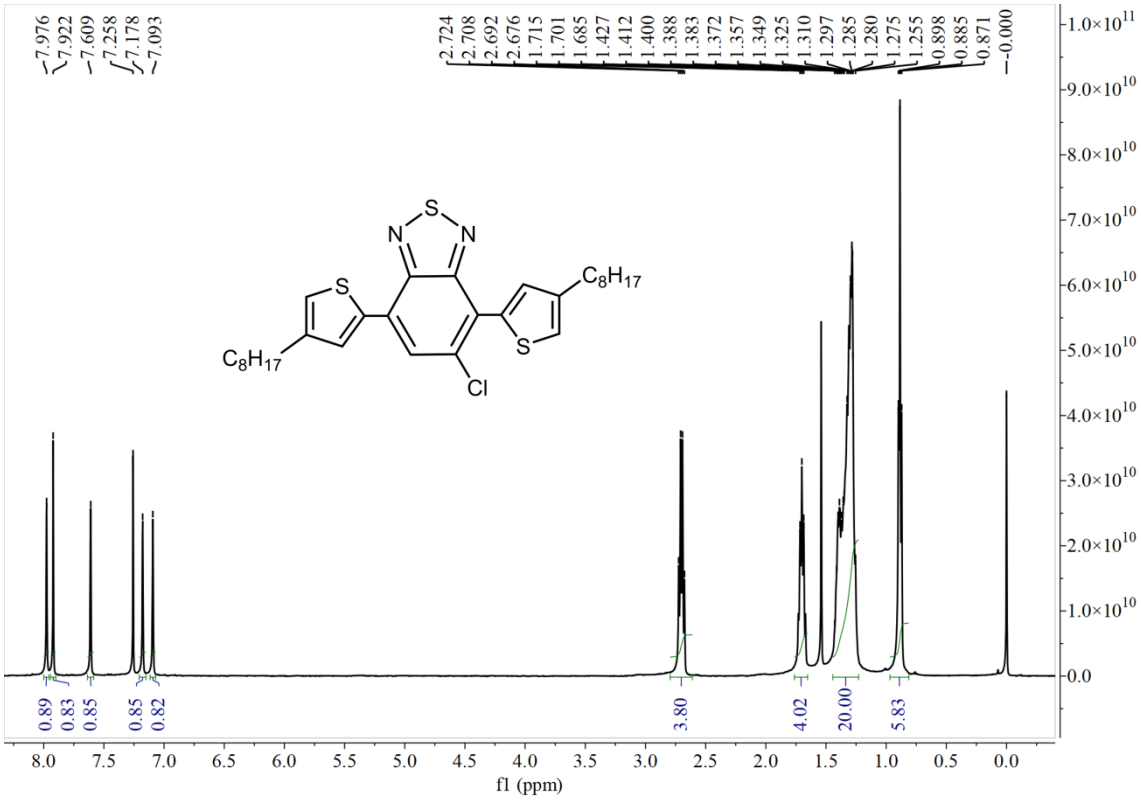

Fig. S8. ^{1}H NMR spectrum of DTClBT in $CDCl_3$.

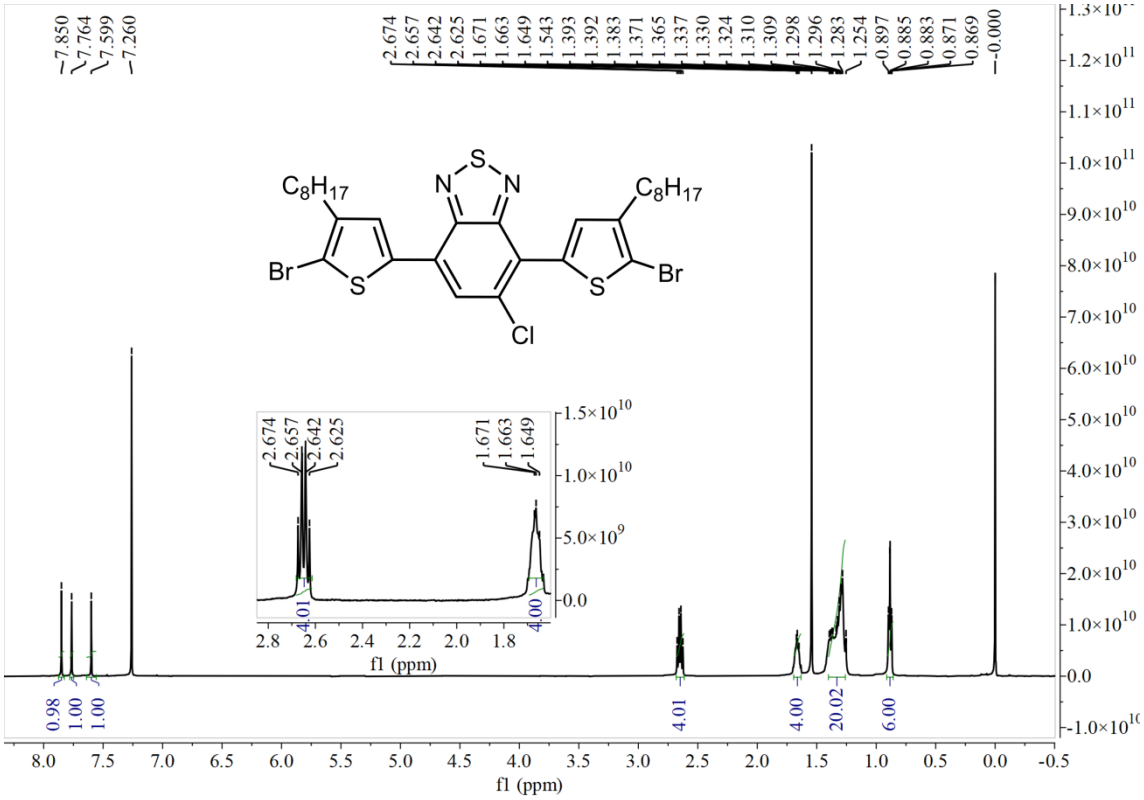

Fig. S9. ^{1}H NMR spectrum of $DTClBTBr_2$ in $CDCl_3$.

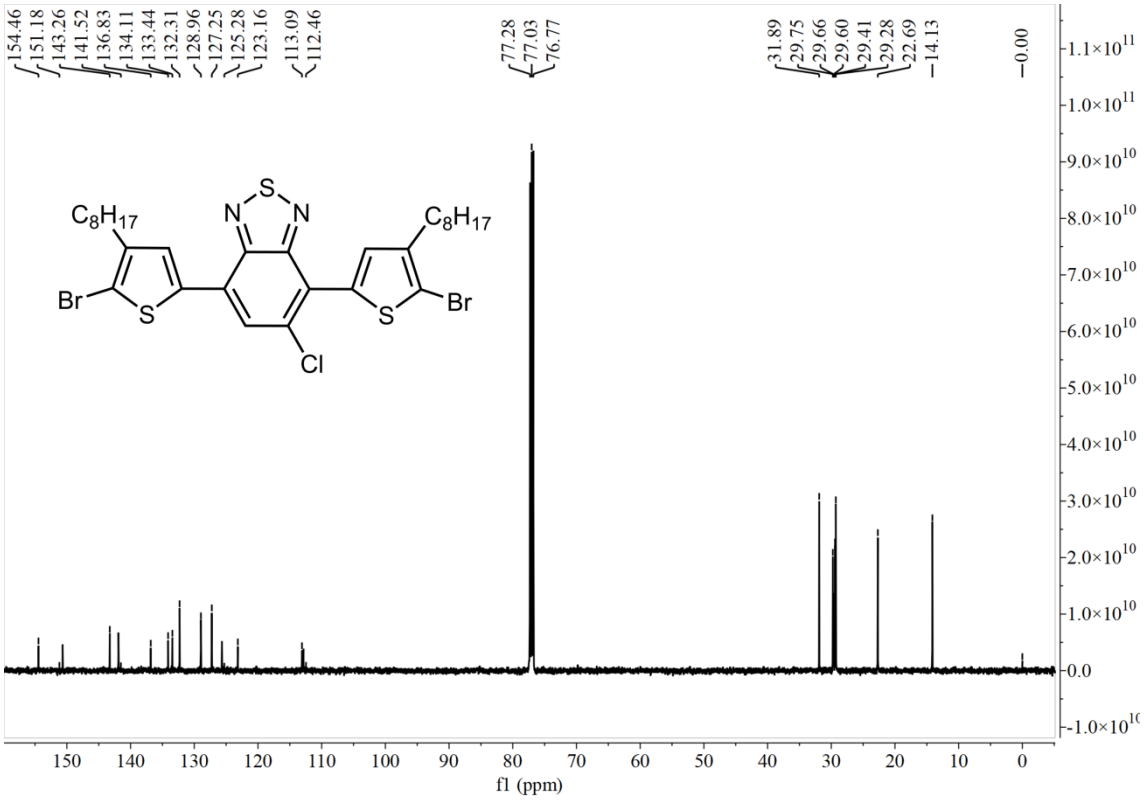

Fig. S10. ^{13}C NMR spectrum of DTClBTBr$_2$ in CDCl$_3$.

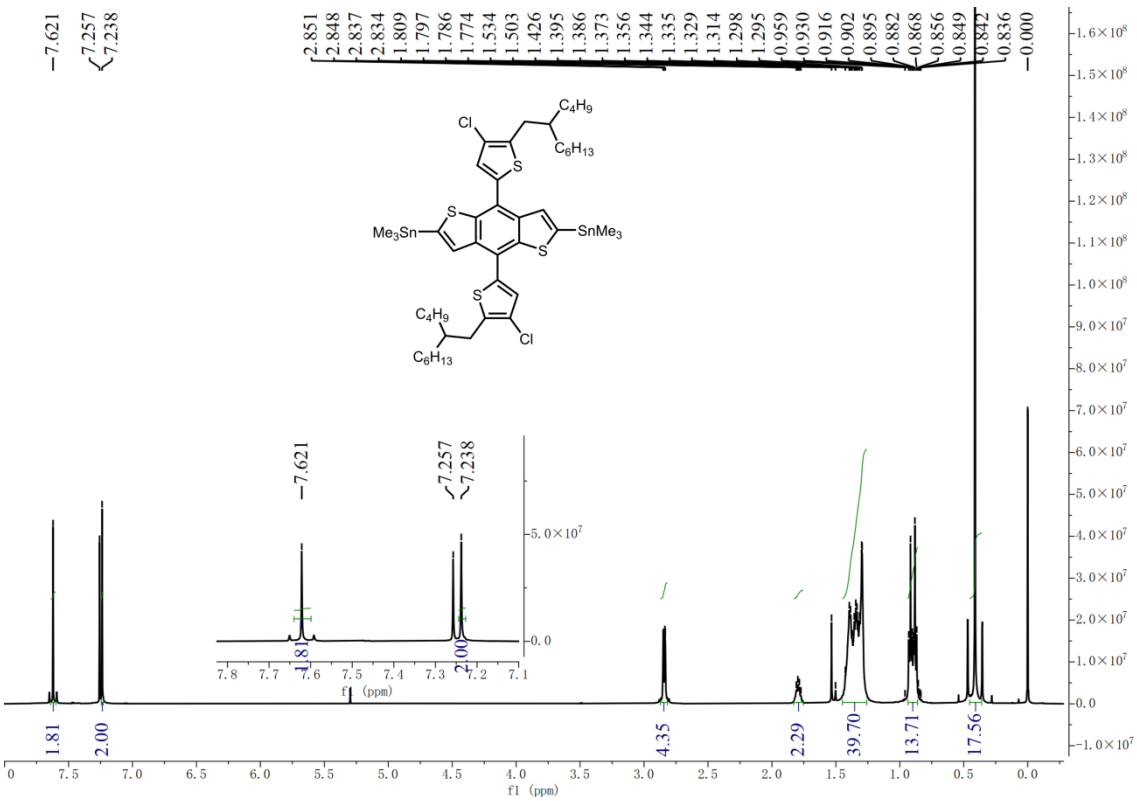

Fig. S11. ^{1}H NMR spectrum of ClBDTSn in CDCl$_3$.

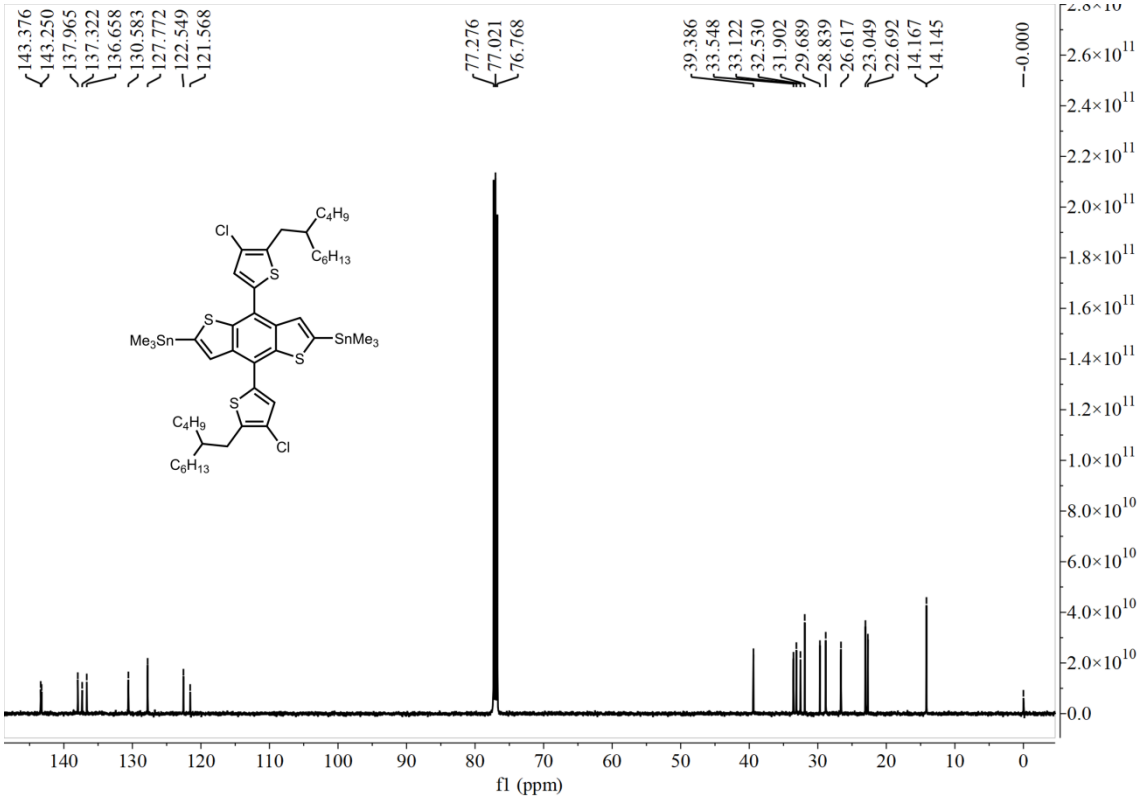

Fig. S12. ^{13}C NMR spectrum of ClBDTSn in $CDCl_3$.

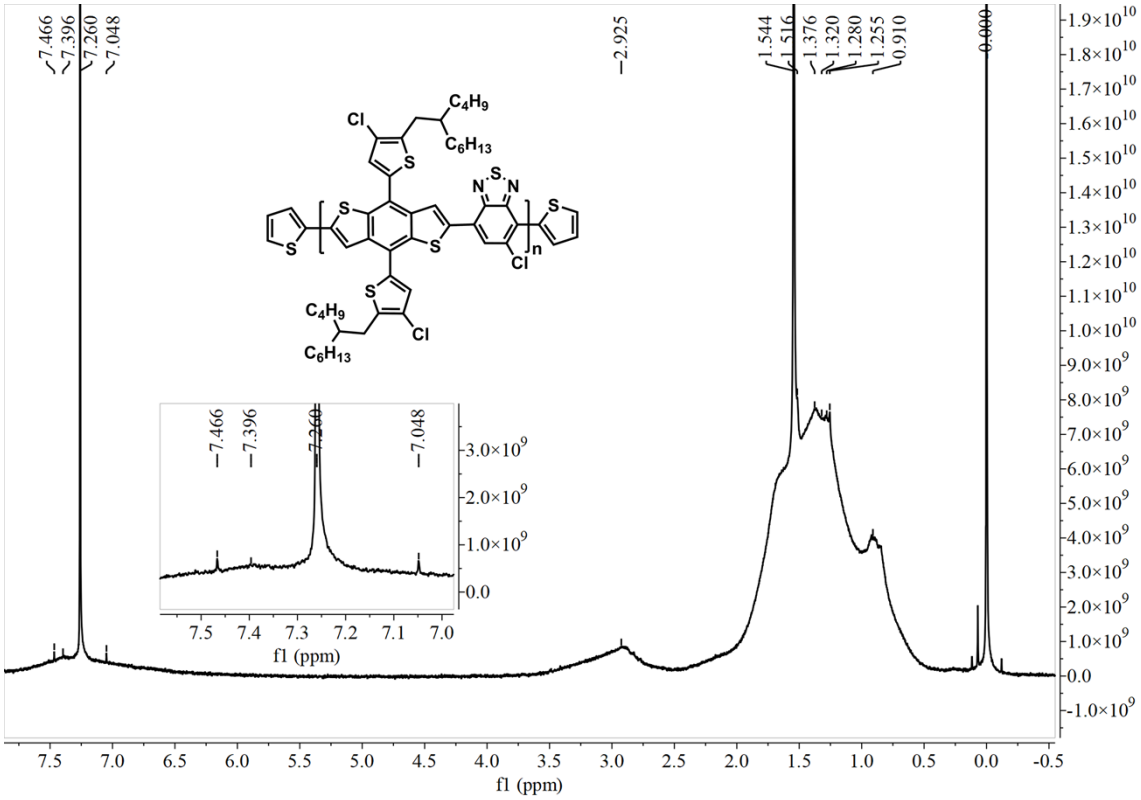

Fig. S13. ^{1}H NMR spectrum of PClBDT-ClBT in $CDCl_3$.

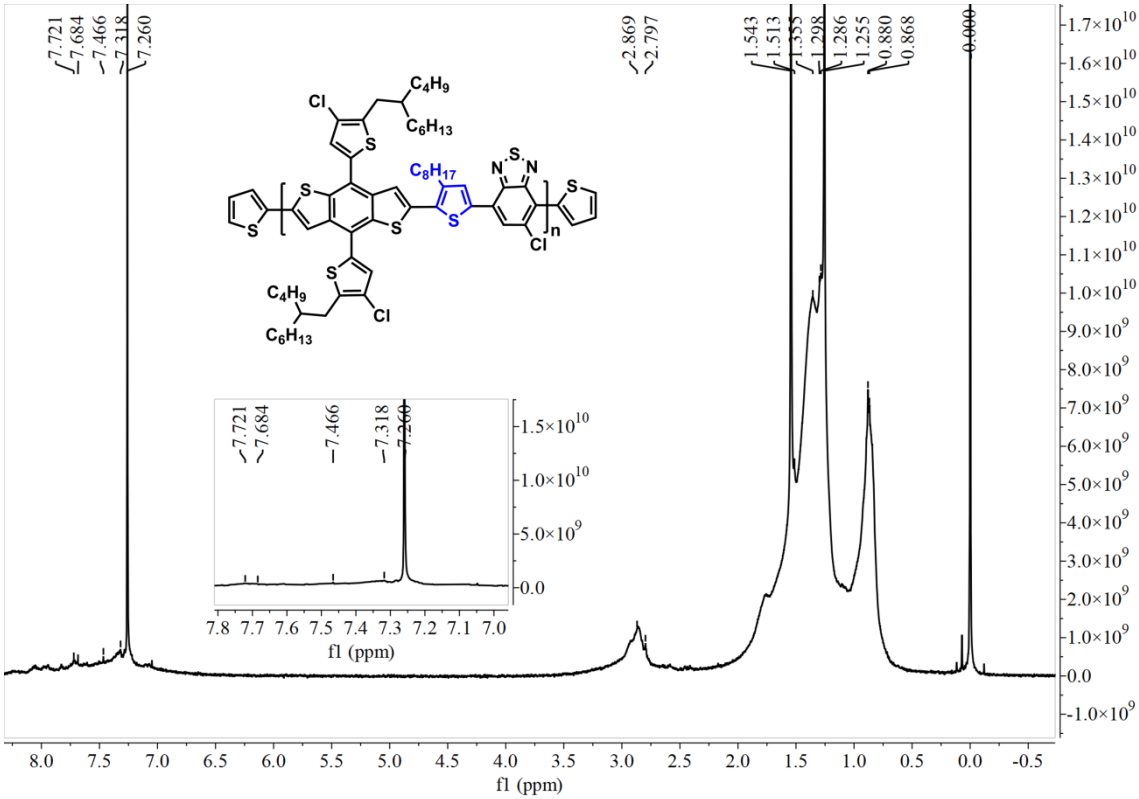

Fig. S14. ^{1}H NMR spectrum of PClBDT-TClBT in $CDCl_3$.

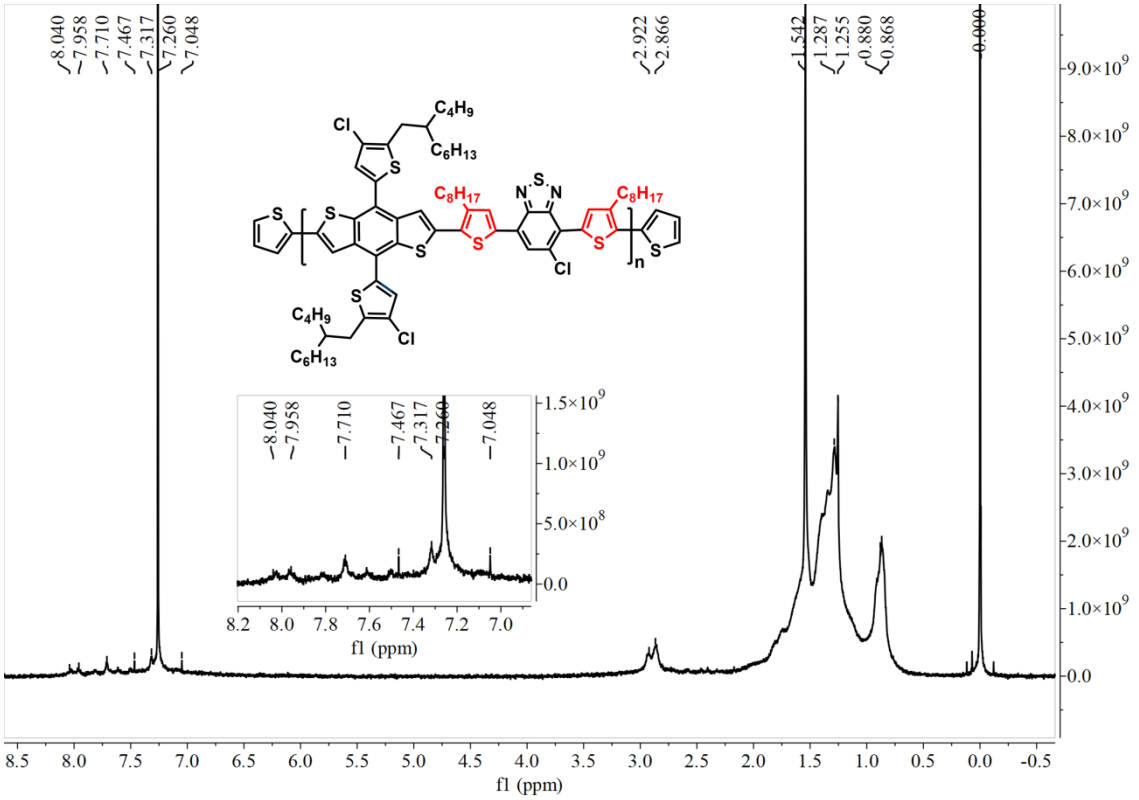

Fig. S15. ^{1}H NMR spectrum of PClBDT-DTClBT in $CDCl_3$.

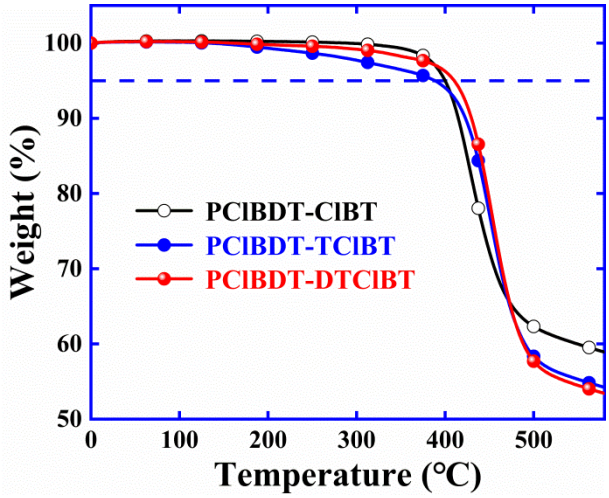

Fig. S16. TG curve of monochlorinated BT-based copolymers PClBDT-ClBT, PClBDT-TClBT and PClBDT-DTClBT.

Table S2. Yield, GPC, TG data of A-A type polymer acceptors PClBDT-ClBT, PClBDT-TClBT and PClBDT-DTClBT.

Polymer	Yield (%)	M_n (kDa)	M_w (kDa)	PDI	T_d (°C)	ε (M^{-1} cm^{-1})
PClBDT-ClBT	93	20.7	40.4	1.95	400	2.83×10^4 (λ=648 nm)
PClBDT-TClBT	93	23.0	51.8	2.25	388	2.95×10^4 (λ=597 nm)
PClBDT-DTClBT	92	24.7	53.1	2.15	410	3.39×10^4 (λ=588 nm)

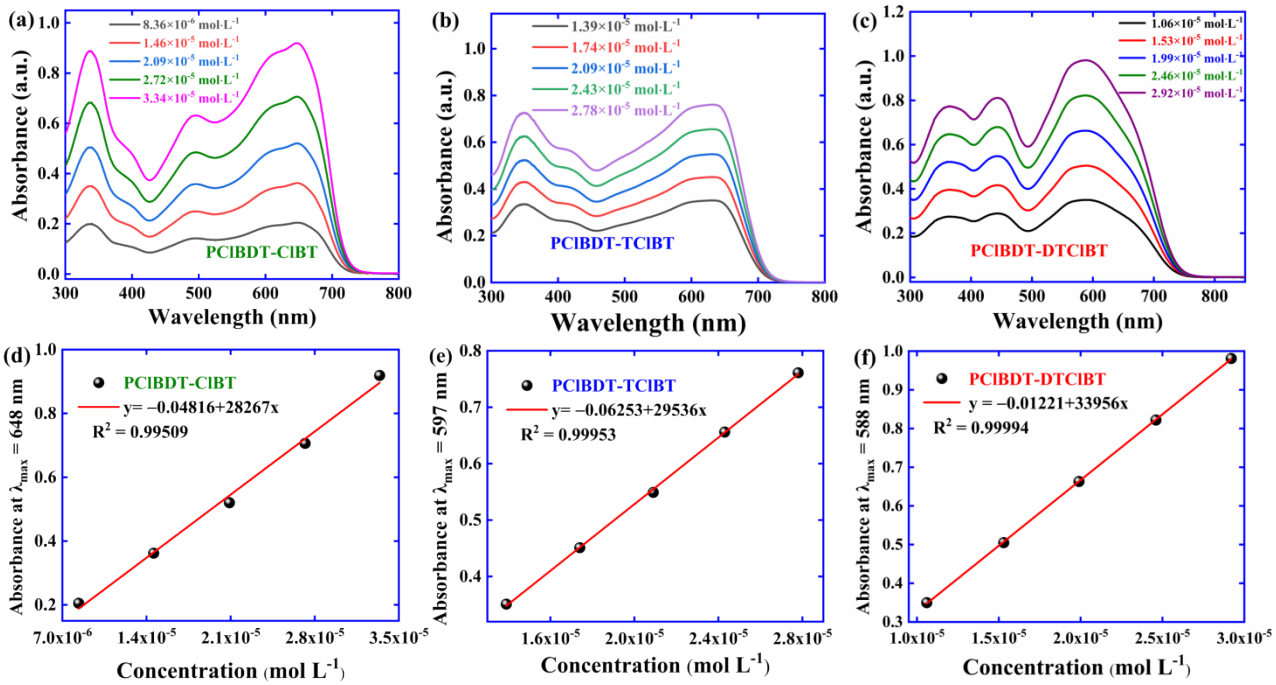

Fig. S17. UV-vis absorption spectra for PClBDT-ClBT, PClBDT-TClBT and PClBDT-DTClBT dissolved in solution at varied concentrations (a, b, c) and the corresponding absorption coefficients (d, e, f).

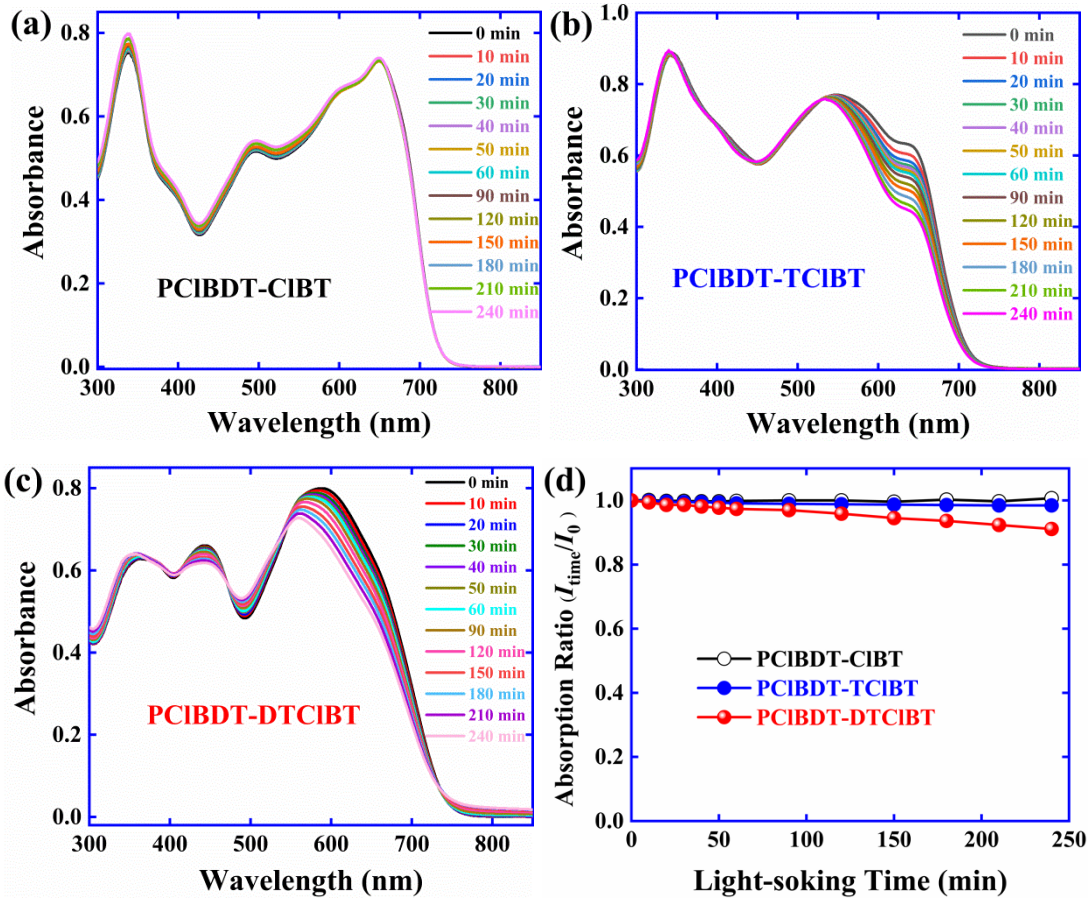

Fig. S18. Absorption variation versus light-soaking time of PClBDT-ClBT (a), PClBDT-TClBT (b), PClBDT-DTClBT (c) and their comparison variation (d) in chlorobenzene.

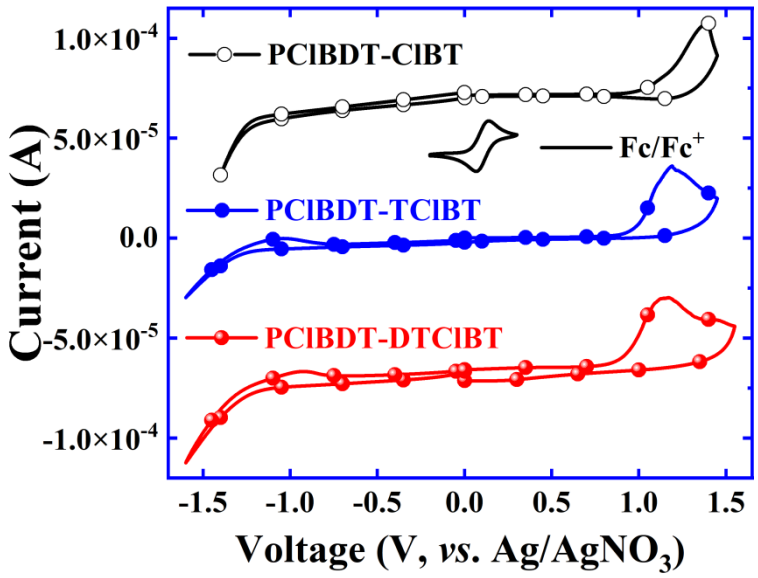

Fig. S19. CV curves for PClBDT-ClBT, PClBDT-TClBT and PClBDT-DTClBT.

Table S3. Dihedral angles of the model molecules $(ClBDT\text{-}ClBT)_2$, $(ClBDT\text{-}TClBT)_2$ and $(ClBDT\text{-}DTClBT)_2$.

Model molecule	Structure	Dihedral angle (deg)
$(ClBDT\text{-}ClBT)_2$	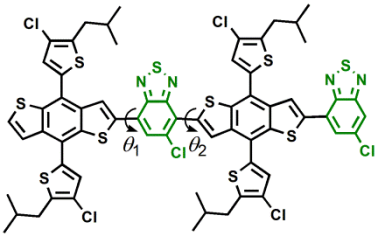	$\theta_1 = -178.33$, $\theta_2 = -143.97$,
$(ClBDT\text{-}TClBT)_2$	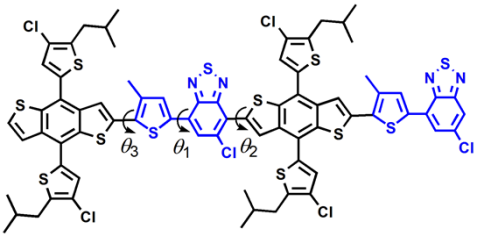	$\theta_1 = -177.53$, $\theta_2 = -147.94$, $\theta_3 = 163.89$,
$(ClBDT\text{-}DTClBT)_2$	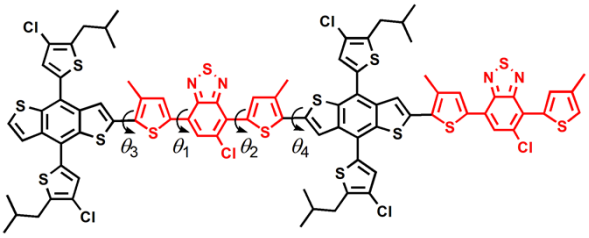	$\theta_1 = -176.32$, $\theta_2 = 156.70$, $\theta_3 = 152.62$, $\theta_4 = 166.77$.

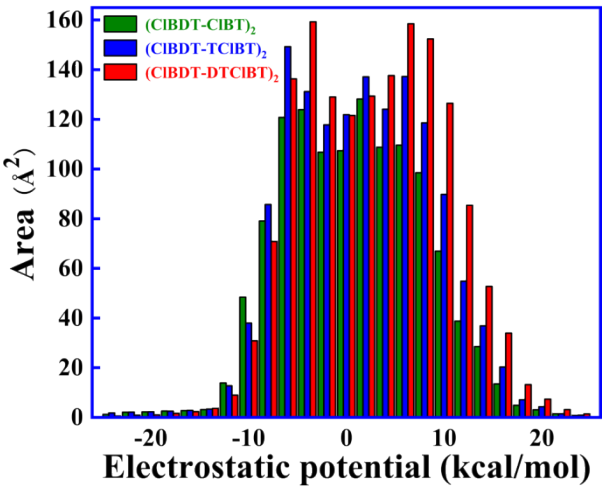

Fig. S20. ESP area distribution of $(ClBDT\text{-}ClBT)_2$, $(ClBDT\text{-}TClBT)_2$ and $(ClBDT\text{-}DTClBT)_2$.

Table S4. Molecular surface area, MPI extremes of ESP and total average ESP of $(ClBDT\text{-}ClBT)_2$ and $(ClBDT\text{-}TClBT)_2$ and $(ClBDT\text{-}DTClBT)_2$ and accepter Y6.

Model Molecules	overall surface area (Å^2)	MPI (kcal/mol)	minimal value (kcal/mol)	maximal value (kcal/mol)	overall average value (kcal/mol)
$(ClBDT\text{-}ClBT)_2$	1217.36	5.98	–24.32	25.21	1.43
$(ClBDT\text{-}TClBT)_2$	1404.13	5.97	–24.91	24.33	1.47
$(ClBDT\text{-}DTClBT)_2$	1568.55	6.20	–26.56	23.80	1.22
Y6	804.65	11.68	–33.41	39.69	5.07

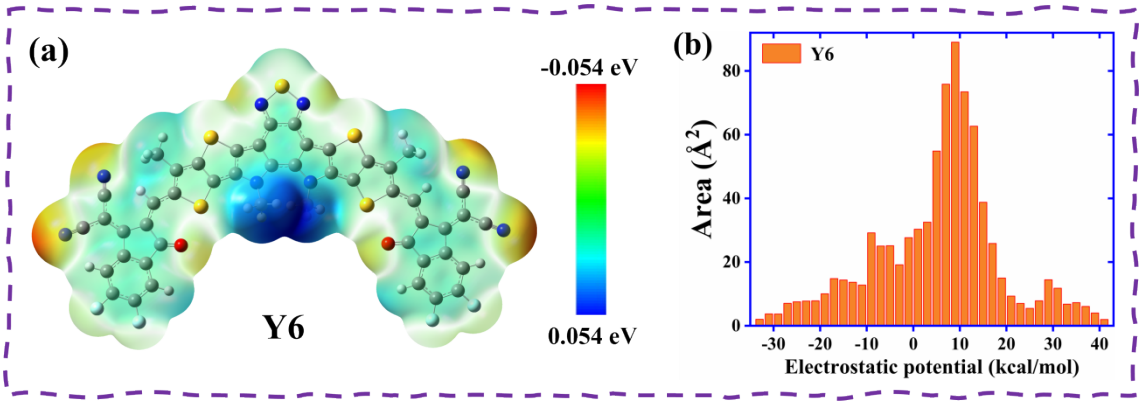

Fig. S21. ESP distribution (a) and ESP area distribution (b) of Y6.

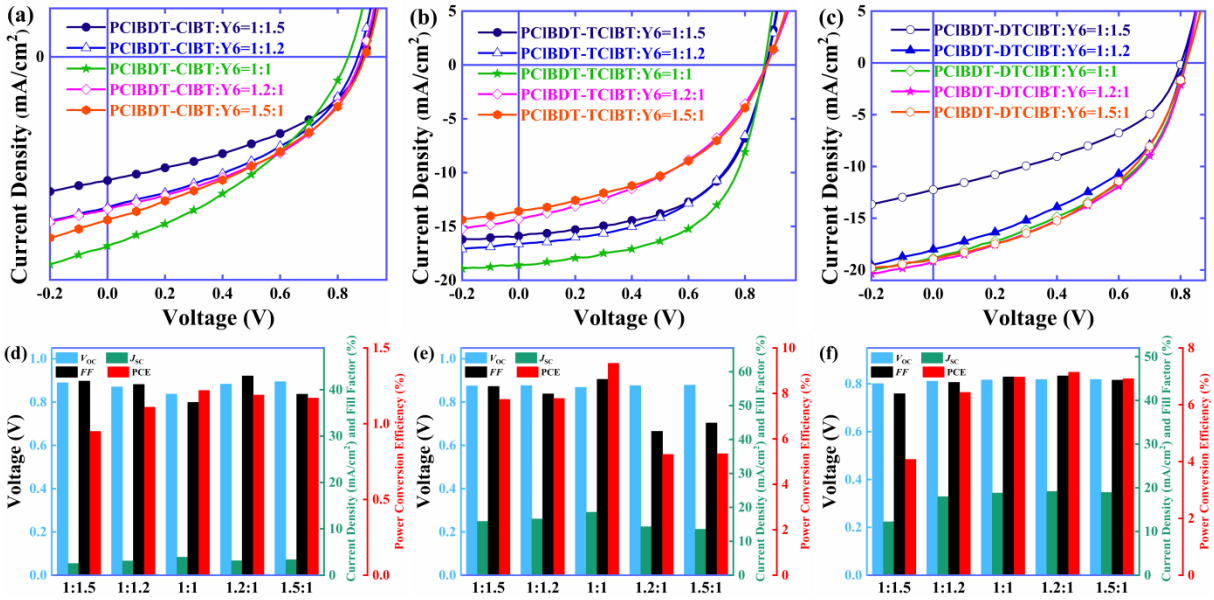

Fig. S22. *J-V* curves of devices based on PClBDT-ClBT (a, d), PClBDT-TClBT (b, e) and PClBDT-DTClBT (c, f) at different weight ratios.

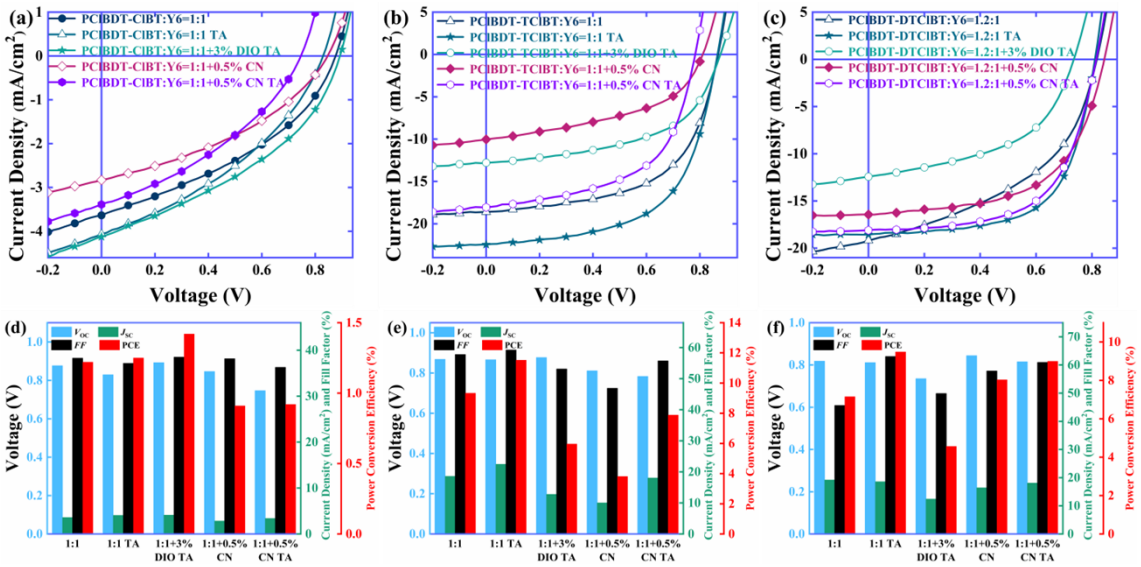

Fig. S23. *J-V* curves of devices based on PClBDT-ClBT (a, d), PClBDT-TClBT (b, e) and PClBDT-DTClBT (c, f) using thermal annealing and solvent additive DIO and CN.

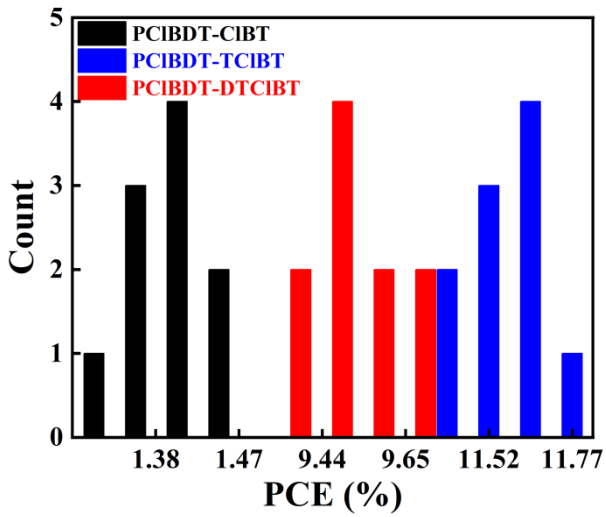

Fig. S24. Histogram statistics of devices based on PClBDT-ClBT, PClBDT-TClBT and PClBDT-DTClBT.

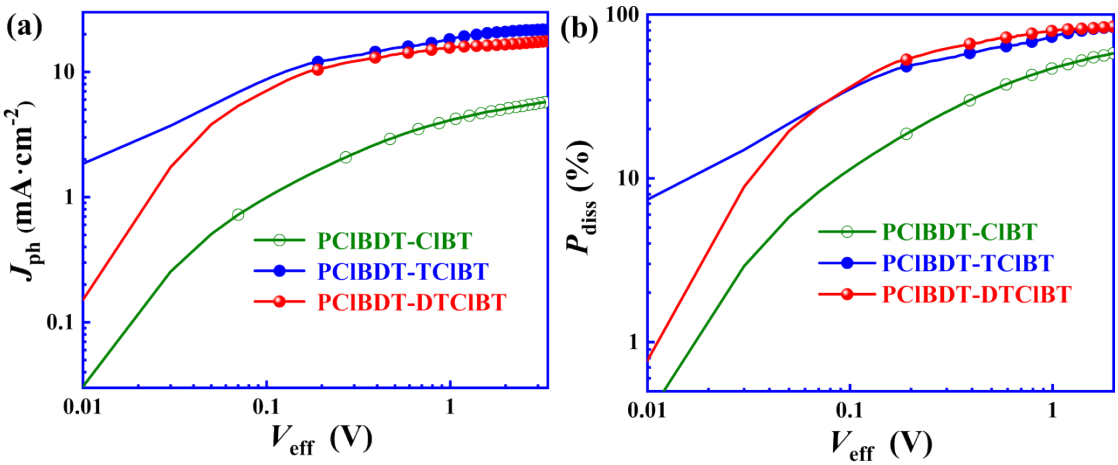

Fig. S25. (a) J_{ph} versus V_{eff} and (b) P_{diss} versus V_{eff} curves for PClBDT-ClBT:Y6-, PClBDT-TClBT:Y6-

and PClBDT-DTClBT:Y6-based devices.

Table S5. Photovoltaic parameters of PClBDT-ClBT, PClBDT-TClBT and PClBDT-DTClBT-based devices.

Polymer Donor	D:A Ratio/Additive	V_{OC} (V)	J_{SC} (mA cm^{-2})	*FF* (%)	PCE (%)
PClBDT-ClBT	1:1.5	0.89	2.55	41.85	0.95
	1:1.2	0.87	3.10	41.13	1.11
	1:1	0.88	3.63	38.28	1.22
	1.2:1	0.88	3.14	42.96	1.19
	1.5:1	0.89	3.37	39.02	1.17
	1:1/TA	0.83	4.07	37.15	1.25
	1:1/3%DIO+TA	0.89	4.12	38.50	1.42
	1:1/0.5%CN	0.85	2.83	38.16	0.91
	1:1/0.5%CN+/TA	0.75	3.39	36.29	0.92
PClBDT-TClBT	1:1.5	0.88	15.89	55.65	7.74
	1:1.2	0.88	16.62	53.45	7.78
	1:1	0.87	18.60	57.76	9.33
	1.2:1	0.88	14.32	42.42	5.32
	1.5:1	0.88	13.58	44.88	5.35
	1:1/TA	0.87	22.45	59.21	11.52
	1:1/3%DIO+TA	0.88	12.79	53.10	5.96
	1:1/0.5%CN	0.81	10.03	46.90	3.81
	1:1/0.5%CN+TA	0.78	18.06	55.71	7.88
PClBDT-DTClBT	1:1.5	0.80	12.24	41.53	4.08
	1:1.2	0.81	18.00	44.12	6.44
	1:1	0.82	18.84	45.37	6.98
	1.2:1	0.82	19.18	45.61	7.15
	1.5:1	0.82	18.96	44.64	6.92
	1.2:1/TA	0.81	18.57	62.99	9.48
	1.2:1/3%DIO+TA	0.74	12.43	49.88	4.56
	1.2:1/0.5%CN	0.84	16.44	57.87	8.03
	1.2:1/0.5%CN+TA	0.82	18.10	60.93	8.99

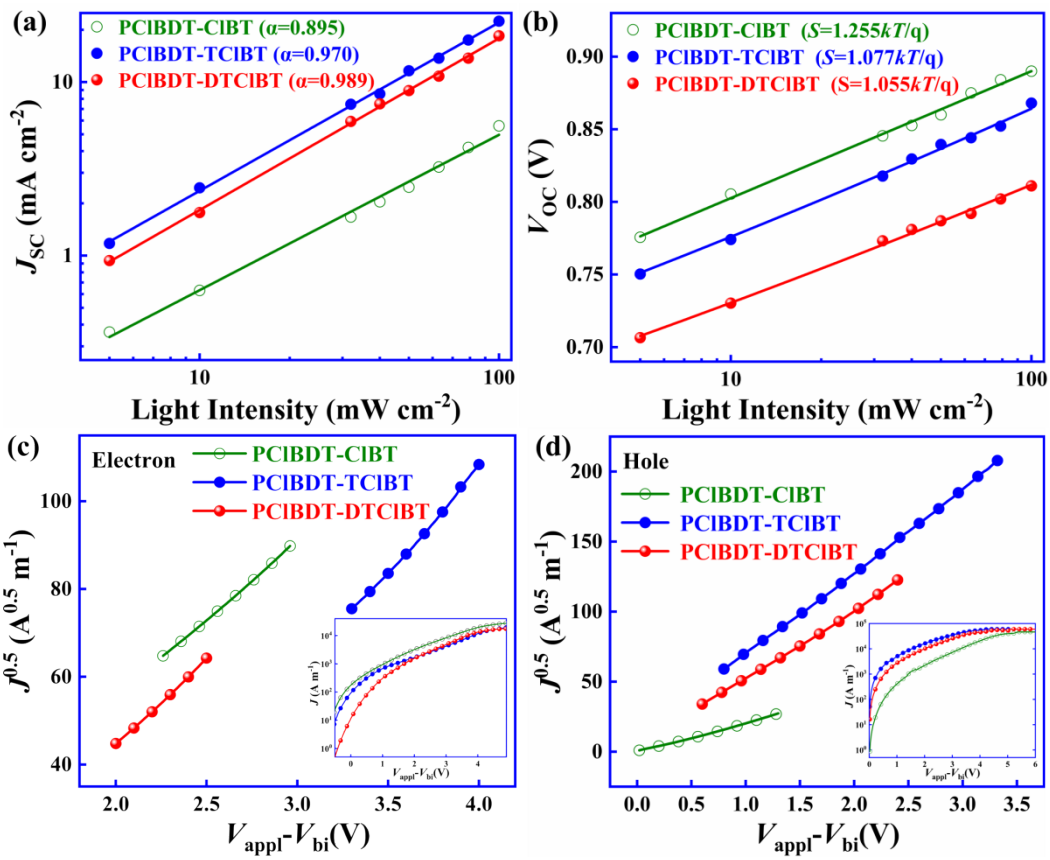

Fig. S26. Plots of J_{SC} (a) and V_{OC} (b) versus light intensity, $J^{0.5}$-V curves of electron-only (c) and hole-only (d) devices under the best fabrication condition.

Table S6 Hole- and electron-motilities of the optimized devices.

Active Layers	k_h	Thickness (nm)	μ_h (cm^2 V^{-1}	k_e	Thickness (nm)	μ_e (cm^2 V^{-1} s^{-1})	μ_h/μ_e
PClBDT-ClBT:Y6	58.92	90	1.06×10^{-4}	28.38	89	1.90×10^{-4}	0.558
PClBDT-TClBT:Y6	54.69	111	1.59×10^{-3}	47.03	113	1.07×10^{-3}	1.486
PClBDT-DTClBT:Y6	21.73	115	1.52×10^{-3}	44.90	115	1.03×10^{-3}	1.476

Table S7 Contact angle, surface tension and interaction parameters of PClBDT-ClBT, PClBDT-TClBT, PClBDT-DTClBT and Y6.

Film	Water (°)	EG (°)	γ (mN/m)	$\chi^{donor\text{-}acceptor}$
PClBDT-ClBT	106.0	79.4	24.03	0.6608K
PClBDT-TClBT	105.4	77.6	25.97	0.3829K
PClBDT-DTClBT	105.2	77.2	26.32	0.3418K
Y6	104.0	72.3	32.66	

Table S8 Experimental data obtained from the GIWAXS characterization

Films	Out of plane (010)				In plane (100)			
	Location (Å^{-1})	d-spacing (Å)	FWHM	CCL_π (Å)	Location (Å^{-1})	d-spacing (Å)	FWHM	CCL_L (Å)
PClBDT-ClBT:Y6	1.734	3.62	0.332	17.03	0.278	22.60	0.0857	65.99
PClBDT-TClBT:Y6	1.697	3.70	0.421	13.43	0.283	22.20	0.1710	33.07
PClBDT-DTClBT:Y6	1.691	3.72	0.404	14.00	0.254	24.74	0.0769	73.54

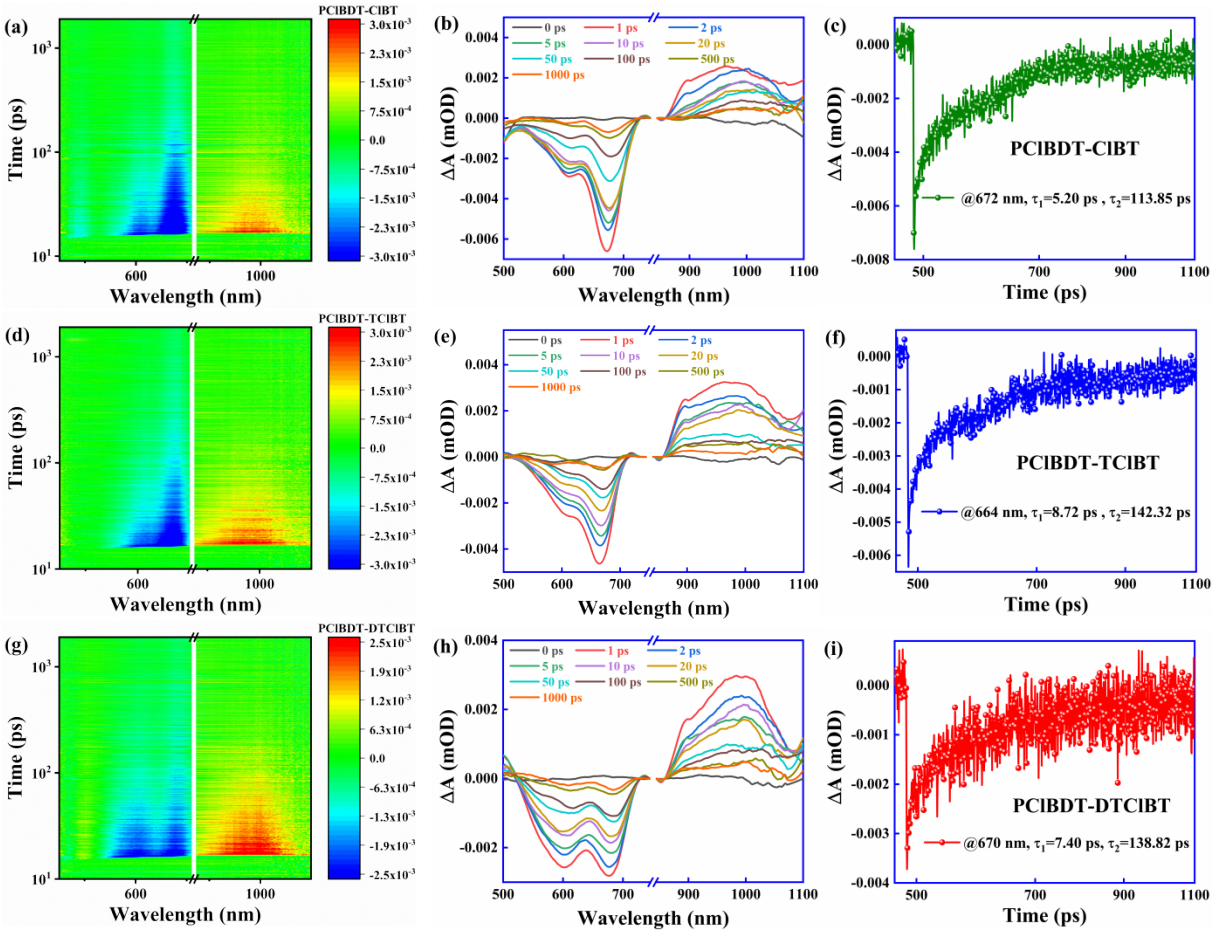

Fig. S27. fs-TA spectra for PClBDT-ClBT (a, b), PClBDT-TClBT (d, e) and PClBDT-DTClBT (g, h) excited at 400 nm. Kinetics processes for PClBDT-ClBT (c) at 672 nm, PClBDT-TClBT (f) at 664 nm and PClBDT-DTClBT (i) at 670 nm.

Reference

(1) D. Mo, H. Wang, H. Chen, S. Qu, P. Chao, Z. Yang, L. Tian, Y.-A. Su, Y. Gao, B. Yang, W. Chen, F. He, *Chem. Mater.*, 2017, **29**, 2819–2830.

(2) Z. Hu, H. Chen, J. Qu, X. Zhong, P. Chao, M. Xie, W. Lu, A. Liu, L. Tian, Y.-A. Su, W. Chen, F. He, *ACS Energy Lett.*, 2017, **2**, 753–758.

(3) Z. Yang, H. Chen, H. Wang, D. Mo, L. Liu, P. Chao, Y. Zhu, C. Liu, W. Chen, F. He, *Polym. Chem.*, 2018, **9**, 940–947.

(4) T. Olla, O. A. Ibraikulov, S. Ferry, O. Boyron, S. Mery, B. Heinrich, T. Heiser, P. Leveque, N. Leclerc, *Macromolecules*, 2019, **52**, 8006－8016.

(5) Y. Zhou, Y. Qin, C. Ni, Y. Xie, *J. Appl. Polym. Sci.*, 2020, **137**, e49006.